

Nuclear-Data Experimental Programs at GSI

Karl-Heinz Schmidt

Gesellschaft für Schwerionenforschung (GSI), Planckstraße 1, 64291 Darmstadt, Germany

Abstract. At GSI, Darmstadt, an extended series of measurements on nuclear-reaction products has been performed. The work is based on an innovative experimental approach, which exploits the unique installations of GSI: The accelerator complex provides heavy-ion beams at relativistic energies, while a high-resolution magnetic spectrometer is used to identify the reaction products in-flight and to determine their kinematical properties. The storage ring extends the facility to a unique place for determining the ground-state masses of exotic nuclei on large areas of the chart of the nuclides.

INTRODUCTION

Intense efforts for systematically providing nuclear data have a long tradition. Right after the discovery of nuclear fission, the determination of neutron-capture cross sections of different materials and the yields of prompt and delayed fission neutrons established the basic knowledge for the development of nuclear technology. Practically all nuclear data, important for the design of conventional fission reactors, have been experimentally determined. Plans for modern developments like the accelerator-driven system (ADS) changed the situation drastically: Due to the extension of the energy range up to 1 GeV, it has become impossible to provide all relevant nuclear data by dedicated experiments. Instead, a different approach has to be taken, according to which some experiments provide key information for a number of well selected cases, which are used for developing appropriate codes, for covering the whole field. Therefore, these experiments should not only provide high-quality data but also enable a very good understanding of the physics.

In this extended sense of research on nuclear data, a number of experimental programs have been carried out at the GSI heavy-ion facility during the last years. The installations of GSI provide unique conditions for experiments in inverse kinematics, which overcome many limitations of conventional experiments. The experiments aimed for measuring complete nuclide distributions, establishing the reaction kinematics and determining ground-state masses in regions which were not accessible before.

THE GSI FACILITY

The installations of the GSI heavy-ion facility, which are essential for the experiments presented in this contribution, are schematically shown in Fig. 1. The beam from the ion source is injected into the UNILAC linear accelerator and leaves it with an energy of 12 A MeV. The SIS heavy-ion synchrotron accelerates it further up to about 1 A GeV. A target for the production of secondary beams is mounted at the entrance of the spectrometer FRS. The FRS and the storage ring ESR allow for studying the reaction products in-flight. The FRS serves as a high-resolution magnetic spectrometer and as a separator for radioactive beams, respectively, in the different experiments. The experimental storage ring ESR stores the ions and serves as a kind of trap for the high-energy ions.

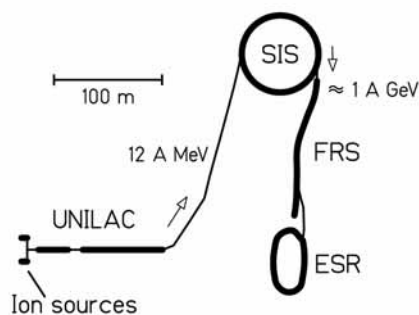


FIGURE 1. Installations of the heavy-ion facility GSI used in the experiments presented in this contribution.

EXPERIMENTAL APPROACHES

Nuclide Identification

After being monitored [1], the primary-beam impinges on the target. The reaction products are separated and identified in the fragment separator FRS [2] and the associated detector equipment, shown in Fig. 2. The FRS is a two-stage magnetic spectrometer with a dispersive intermediate image plane (S_2) and an achromatic final image plane (S_4). The acceptance of the fragment separator is about 3 % in momentum and 15 mr in angle around the beam axis. Two position-sensitive plastic-scintillation detectors [3], placed at S_2 and S_4 , provide the magnetic rigidities ($B\rho$) and the time-of-flight measurements.

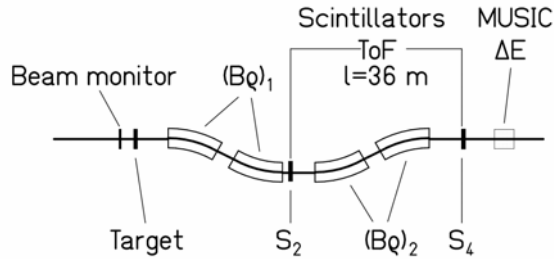


FIGURE 2. Schematic drawing of the fragment separator and of the detector equipment.

The mass-over-charge ratio is determined from the equation

$$\frac{M(A, Z)}{Z} = \frac{B\rho e}{\gamma v} \quad (1)$$

where $M(A, Z)$ is the mass of the nucleus with atomic number Z and mass number A , v is the velocity, γ the Lorentz factor, and e the elementary charge. The nuclear charge is identified using an ionization chamber (MUSIC) [4]. The mass resolving power $A/\Delta A=400$ is sufficient to identify all reaction products unambiguously.

High-Resolution Momentum Measurements

Once the reaction residue is identified, the measurement of its magnetic rigidity, deduced from the horizontal position at the intermediate dispersive image plane of the fragment separator, gives precise information on its longitudinal momentum. Measure-

ments with different magnetic fields are combined to fully cover the momentum distributions of the residues. The momentum of individual reaction products is determined with a relative uncertainty of $\pm 5 \cdot 10^{-4}$, which is about an order of magnitude more precise than the time-of-flight measurement performed with the scintillation detectors on a flight path of 36 m.

Mass Measurements

Radioactive isotopes from the production target mounted in front of the fragment separator and pre-selected by the separator are injected into the experimental storage ring ESR [5]. The ground-state masses are determined with a resolving power of about $2 \cdot 10^6$ by two different methods.

Schottky Mass Spectrometry

The revolution frequencies of electron-cooled circulating ions in the ESR are measured by the non-destructive Schottky-diagnosis technique [6]. Due to the necessary cooling and measuring time only nuclei with half-lives larger than 30 s can be investigated.

Isochronous Mass Spectrometry

The revolution times of the ions in the ESR are measured with a dedicated timing detector with extremely high time resolution [7]. For this method, the storage ring is operated on transition and no cooling of the ion beam is required. Thus, masses of nuclides with half-lives as short as 10 μ s are obtained.

RESULTS

Systematic Determination of Nuclear Masses

Time-resolved Schottky Mass Spectrometry

Direct measurements of projectile fragments with the time-resolved Schottky Mass Spectrometry (SMS) [8] have been applied for systematic mass determinations on relatively long-lived neutron-deficient nuclei, which are linked to stable nuclei only by beta decay. The achieved mass accuracy was typically 30 keV. In addition, the masses of a large number of additional

nuclides were indirectly determined by means of known decay energies (α , β or proton). The measured masses cover a large area of neutron-deficient nuclides from krypton to uranium (see Fig. 3). The data were included in the latest Atomic Mass Evaluation (AME) [9].

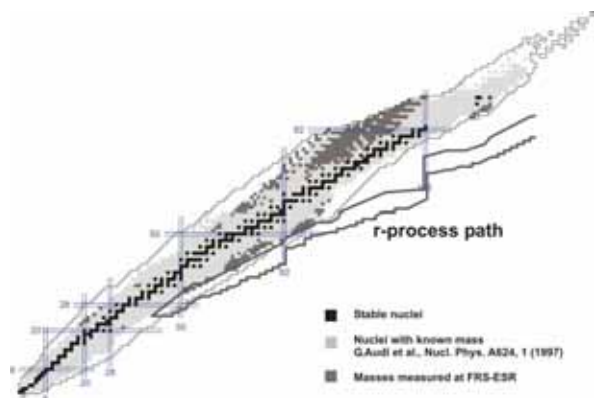


FIGURE 3. Nuclei investigated by mass spectrometry at GSI presented on the chart of the nuclides.

Isochronous Mass Spectrometry

Isochronous Mass Spectrometry (IMS) [10] was used with uranium fission fragments. Masses of 41 short-lived neutron-rich nuclides in the element range of $32 \leq Z \leq 57$ were measured for the first time [11]. A mass resolving power of 2×10^5 (FWHM) was achieved with a typical uncertainty of about 2×10^{-6} . The new masses belong to very exotic nuclides close to the astrophysical r-process path. Thus, they are of great importance for testing the predictive power of current mass models which are extensively used for astrophysical calculations.

Nuclide Distributions

The nuclide distributions¹ of the reaction products from a number of key reactions, $^{238}\text{U} + ^1_2\text{H}$, Ti [12, 13, 14, 15, 16], $^{208}\text{Pb} + ^1_2\text{H}$, Ti [17, 18, 19, 20], $^{197}\text{Au} + ^1_1\text{H}$ [21, 22], $^{136}\text{Xe} + ^1_1\text{H}$ [23], $^{56}\text{Fe} + ^1_1\text{H}$ [23, 24], $^{238}\text{U} + ^{208}\text{Pb}$ [25], $^{136}\text{Xe} + ^{208}\text{Pb}$ [26], mostly at 1 A GeV, but some also at lower beam energies, have been systematically determined. Fig. 4 shows the nuclide distribution for the system $^{238}\text{U} + ^1_1\text{H}$ at 1 A GeV as an example. The two regions, populated by spallation-evaporation (above dysprosium) and spallation-fission reactions (up to dysprosium) are clearly seen.

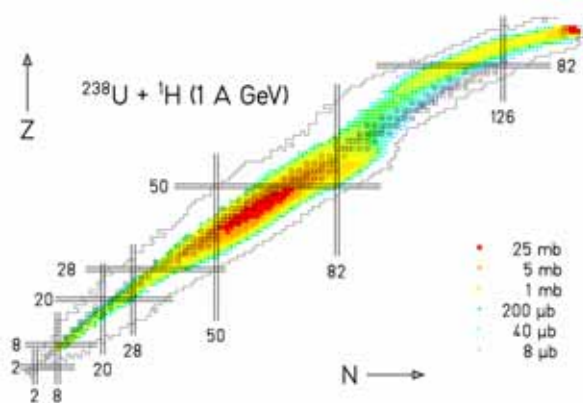


FIGURE 4. Measured nuclide cross sections from the reaction $^{238}\text{U} + ^1_1\text{H}$ at 1 A GeV on the chart of the nuclides. The color code gives the cross sections according to the indicated scale.

This is the first time that practically complete nuclide and velocity distributions in fragmentation reactions of heavy nuclei were determined. Conventional experiments, which relied on gamma-spectroscopic measurements of targets or catchers, irradiated by high-energy projectiles, could determine the independent yields of only some specific nuclei in an adapted half-life range prior to radioactive decay.

These results are relevant for deducing the nuclide production induced in the bombardment of the converter target and other construction material in an ADS, important e.g. for shielding and long-term radioactive inventory. They also represent a valuable basis for benchmarking and improving nuclear-reaction codes.

The kinematical properties of the reaction products are relevant for the radiation damage induced in construction material due to the exposure to high-energy particles. Some more fundamental aspects on the properties of nuclear matter which are important for a better understanding of nuclear matter and nuclear reactions in general will be discussed below.

Isospin Thermometer

The study of the properties of nuclear matter with extreme N/Z ratio has come into the focus of recent research activities due to its importance for the understanding of supernova explosions and the stability of neutron stars. Many important results have been obtained by detecting light nuclei ($A \leq 20$) in full-acceptance experiments. The systematic results on nuclide distributions in fragmentation reactions, mentioned above, allow extending these investigations to heavier nuclei.

¹ Data tables on this URL: <http://www-w2k.gsi.de/kschmidt>

Fig. 5 shows an overview of the data on the mean neutron-to-proton ratio $\langle N \rangle / Z$ of the isotopic chains measured for two systems. Fragments from projectiles with different N/Z are shifted in their $\langle N \rangle / Z$ values: The residues formed by fragmentation of ^{238}U ($N/Z = 1.587$) are more neutron rich than those formed in the fragmentation of ^{208}Pb ($N/Z = 1.537$).

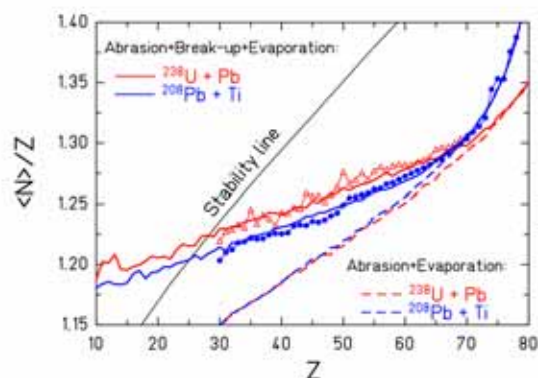


FIGURE 5. Mean neutron number of isotopic distributions divided by Z as a function of the atomic number for the systems $^{238}\text{U} + \text{Pb}$ (open triangles) and $^{208}\text{Pb} + \text{Ti}$ (full points). The data are compared with ABRABLA calculations without a break-up phase and with a break-up phase, using a freeze-out temperature of 5.5 MeV.

These results show that there is a memory of the neutron excess of the projectile found in the projectile fragments over the whole mass range investigated.

In Fig. 5, the $\langle N \rangle / Z$ values of the light fragments from ^{238}U and ^{208}Pb on Ti at 1 A GeV, are also compared with the results of the statistical fragmentation code ABRABLA. The model includes an abrasion stage, where the excited spectator is formed, and a successive de-excitation phase through an evaporation-fission competition. In between these two stages, a break-up stage was introduced, where a heavy fragment is formed along with smaller clusters. The result shows that a good agreement with the data is achieved when the break-up stage is taken into account with a freeze-out temperature of 5.5 MeV. The calculation with a 2-stage abrasion/evaporation model places the final residues on the more neutron-deficient side of the nuclear chart. Consequently, the $\langle N \rangle / Z$ of the final products carries information on the temperature at the beginning of the evaporation cascade, thus establishing the method of the isospin thermometer [27].

Recently, high-precision data on invariant cross sections have shown that break-up has to be considered also in the interactions between protons and light nuclei, e.g. iron, at 1 A GeV [28], what can be essential

for the applications in nuclear technology and astrophysics.

Structural Effects in the Superfluid Phase

The yield distributions of the residues produced in high-energy fragmentation reactions show a pronounced fine structure. Due to the full identification of the residues over extended regions of the chart of the nuclides, this effect could be studied for the first time in its full complexity. Fig. 6 shows the yields of the light residues from the reaction $^{238}\text{U} + \text{Ti}$ as an example [29]. Chains of even-mass nuclei show an enhanced production of even- Z nuclei, while an enhanced production of odd- Z nuclei is observed in odd-mass nuclei. The chain $N=Z$ shows the strongest even-odd effect, while the chain $N-Z=5$ shows the strongest reversed even-odd effect. Most features of these results are reproduced by statistical evaporation calculations [29] and can be interpreted as the result of the condensation process of heated nuclear matter cooling down in the evaporation process. The observed fine structure is the manifestation of the passage from normal liquid phase of the nucleus to its super-fluid phase.

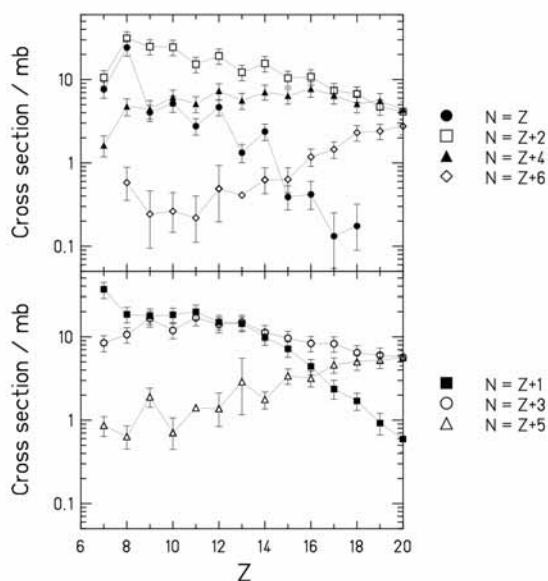


FIGURE 6. Formation cross sections of the projectile-like residues from the reaction $^{238}\text{U} + \text{Ti}$, 1 A GeV. The data are given for chains along even values of $N-Z$ (upper panel) and odd values of $N-Z$ (lower panel).

These findings have important consequences for the prediction of specific nuclide yields, e.g. for nuclide production in the transport of heavy cosmic particles through the interstellar space or for the applica-

tion of isotopic yields for the isotopic-thermometer method [30].

Excitation of the Nucleon in the Nuclear Medium

The momentum distributions of bismuth isotopes, produced by charge-pickup reactions, were determined for the systems $^{208}\text{Pb} + ^{1,2}\text{H}$ at 1 A GeV [20]. Fig. 7 shows the velocity spectrum of the charge-exchange product ^{208}Bi . The high momentum resolution of the FRS allows distinguishing quasi-elastic collisions of a projectile neutron with a target proton from a transformation of a projectile neutron into a proton via the excitation of the $\Delta(1232)$ -resonance, corresponding to an energy transfer of about 400 MeV. The spectra obtained with the two targets show different relative yields for the two processes. They reveal the different characteristics of neutron- and proton-induced collisions with the projectile nucleons.

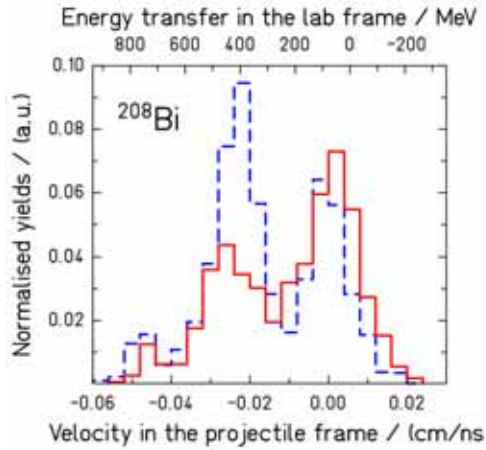


FIGURE 7. Velocity distribution, in the projectile frame, of ^{208}Bi , formed by charge-exchange from ^{208}Pb projectiles in collisions with protons (full histogram) and deuterons (dashed histogram) at 1 A GeV.

Momentum Dependence of the Nuclear Mean Field

The precise measurement of the kinematical properties of the spectators represents a new tool to study the in-medium nucleon-nucleon interactions [31]. This method exploits the direct impact of the participant's expansion on the kinematical properties of the surviving heavy spectator remnants. The mean velocities of the spectator residue measured in reaction $^{238}\text{U}+\text{Ti}$ is

shown in Fig. 8 as a function of the final residue mass. Fission events are excluded.

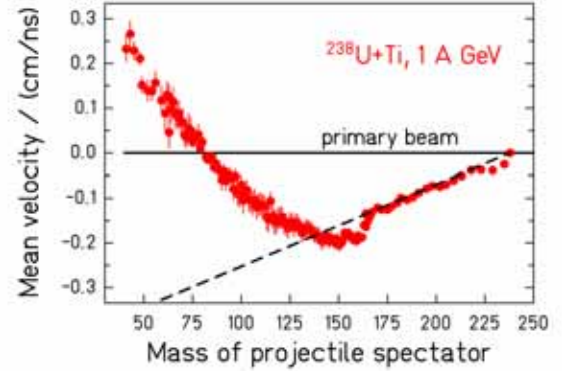


FIGURE 8. Mean values of the velocity distributions of reaction residues, excluding fission, produced in the reaction $^{238}\text{U} + \text{Ti}$ at 1 A GeV in the rest frame of the projectile in comparison with the Morrissey systematics (dashed line). The data are shown as a function of the residue mass.

From Fig. 8 it can be seen that the mean velocity of the heaviest residues, corresponding to the largest impact parameters, decreases with increasing mass loss as given by the Morrissey systematic [32]. However, for the less peripheral collisions, leading to lighter fragments, the velocities of the fragmentation products do not decrease any more. The velocities of the lightest fragments even tend to increase, until finally they become even faster than the projectiles. According to theoretical calculations, this acceleration found for the light reaction residues is a consequence of the momentum dependence of the nuclear mean field [33]. This property is rather unique compared to most experimental signatures, which are sensitive to both the hardness of the EOS and the momentum dependence of the mean field.

Fission

A few additional studies concerning nuclear fission, which are relevant for fission-based nuclear technology, should also shortly be mentioned.

Systematic study of the evolution of fission channels

Using the secondary-beam facility of GSI, a new kind of fission experiment has been performed. Fission properties of short-lived neutron-deficient nuclei, produced as secondary beams, have been investigated in inverse kinematics [34]. The measured element distri-

butions, see Fig. 8, mapped the transition from symmetric to asymmetric fission and extended the systematics of shell structure and even-odd effects [35, 36] and led to an improved understanding of structure effects in nuclear fission.

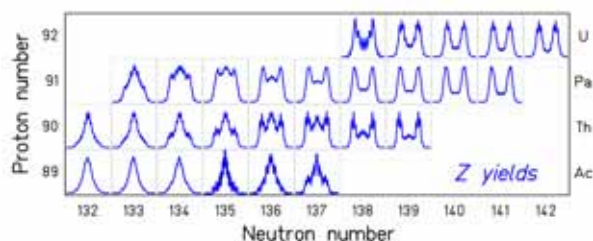


FIGURE 9. Measured fission-fragment element distributions. Fission was induced by electromagnetic excitations of secondary beams at 460 A MeV in a lead target.

Direct insight into transient effects in fission

A new experimental approach has been introduced to investigate the relaxation of the nuclear deformation degrees of freedom [37]. Highly excited fissioning systems with compact shapes and low angular momenta are produced in peripheral relativistic heavy-ion collisions. Both fission fragments are identified in atomic number. Fission cross sections and fission-fragment element distributions are determined as a function of the fissioning element. The comparison of the experimental observables with model calculations indicates that the collective nuclear motion up to the saddle point is critically damped.

ACKNOWLEDGMENTS

This contribution presents the results of many experiments, performed by several groups and collaborations. They comprise the following scientists: P. Armbruster, F. Attallah, L. Audouin, C.-O. Bacri, K. Beckert, P. Beller, J. Benlliure, M. Bernas, B. Berthier, F. Bosch, A. Boudard, D. Boutin, T. Buervenich, E. Casarejos, J. J. Connell, S. Czajkowski, P. Danielewicz, J.-E. Ducret, H. Eickhoff, T. Enqvist, T. Faestermann, M. Falch, B. Fernandez, L. Ferrant, B. Franczak, B. Franzke, H. Geissel, J. S. George, F. Hammache, M. Hausmann, A. Heinz, K. Helariutta, M. Hellström, V. Henzl, D. Henzlova, A. R. Junghans, B. Jurado, D. Karamanis, E. Kaza, A. Kelić, Th. Kerscher, O. Klepper, H.-J. Kluge, R. Koyama, C. Kozhuharov, A. Krása, K.-L. Kratz, R. Legrain, S. Leray, Yu. A. Litvinov, S. A. Litvinov, K. E. G. Löbner, L. Maier, M. Matoš, R. A. Mewaldt, G. Münzenberg, B. Musta-

pha, P. Napolitani, F. Nolden, Yu. N. Novikov, T. Ohtsubo, M. F. Ordonez, A. Ostrowski, A. Ozawa, Z. Patyk, J. Pereira, B. Pfeiffer, M. Pfützner, R. Pleskac, M. Portillo, M. Pravikoff, B. W. Quint, T. Radon, B. Ranjan Behera, F. Rejmund, M. V. Ricciardi, C. Scheidenberger, C. Schmitt, V. Shishkin, C. J. Stadlmann, M. Steck, S. Steinhäuser, C. Stéphan, K. Sümmerner, T. Suzuki, J. Taïeb, L. Tassan-Got, M. B. Trzhakovskaya, S. Typel, D. J. Vieira, C. Villagrasa, F. Vivès, C. Volant, B. Voss, A. Wagner, S. Watanabe, P. Walker, H. Weick, M. E. Wiedenbeck, M. Winkler, W. Wlazole, H. Wollnik, T. Yamaguchi, N. E. Yanasak, and O. Yordanov.

REFERENCES

1. B. Jurado et al., *Nucl. Instr. Meth.* **A 483**, 603 (2002).
2. H. Geissel et al., *Nucl. Instr. Meth.* **B 70**, 286 (1992).
3. B. Voss et al., *Nucl. Instr. Meth.* **A 364**, 150 (1995).
4. M. Pfützner et al., *Nucl. Instr. Meth.* **B 86**, 213(1994).
5. B. Franzke, *Nucl. Instr. Meth.* **B 24**, 18 (1987).
6. B. Schlitt et al., *Hyperfine Interact.* **99**, 117 (1996).
7. J. Trötscher et al., *Nucl. Instr. Meth.* **B 70**, 455 (1992).
8. Yu. A. Litvinov et al., *Nucl. Phys.* **A 734**, 473c (2004).
9. G. Audi et al., *Nucl. Phys.* **A 729**, 337 (2003).
10. M. Hausmann et al., *Nucl. Instr. Meth.* **A 446**, 569 (2000).
11. M. Matos, PhD thesis, JLU Giessen, 2004.
12. J. Taïeb et al., *Nucl. Phys.* **A 724**, 413 (2003).
13. M. Bernas et al., *Nucl. Phys.* **A 725**, 213 (2003).
14. M. V. Ricciardi, *PhD thesis*, Univ. Sant. de Comp, in preparation.
15. E. Casarejos, *PhD thesis*, Univ. Sant. de Comp., 2001.
16. J. Pereira, *PhD thesis*, Univ. Sant. de Comp., 2004.
17. T. Enqvist et al., *Nucl. Phys.* **A 686**, 481 (2001).
18. T. Enqvist et al., *Nucl. Phys.* **A 703**, 435 (2002).
19. B. Fernandez et al., *Nucl. Phys.* **A**, submitted.
20. A. Kelic et al., *Phys. Rev.* **C**, submitted.
21. F. Rejmund et al., *Nucl. Phys.* **A 683**, 540 (2001).
22. J. Benlliure et al., *Nucl. Phys.* **A 683**, 513 (2001).
23. P. Napolitani, *PhD thesis*, Univ. Paris XI, 2004.
24. C. Villagrasa, *PhD thesis*, Univ. Paris XI, 2003.
25. T. Enqvist et al., *Nucl. Phys.* **A 658**, 47 (1999).
26. D. Henzlova, *PhD Thesis*, Czech Techn. Univ. Prague, in preparation.
27. K.-H. Schmidt et al., *Nucl. Phys.* **A 710**, 157 (2002).
28. P. Napolitani et al., *Phys. Rev.* **C**, accepted.
29. M. V. Ricciardi et al., *Nucl. Phys.* **A 733**, 299 (2004).
30. S. Albergo et al., *Nuovo Cimento* **89**, 1 (1985).
31. M. V. Ricciardi et al., *Phys. Rev. Lett.* **90**, 212302 (2003).
32. D. Morrissey, *Phys. Rev.* **C 39**, 460 (1989).
33. L. Shi et al., *Phys. Rev.* **C 64**, 034601 (2001).
34. K.-H. Schmidt et al., *Nucl. Phys.* **A 665**, 221 (2000).
35. S. Steinhäuser et al., *Nucl. Phys.* **A 634**, 89 (1998).
36. F. Rejmund et al., *Nucl. Phys.* **A 678**, 215 (2000).
37. B. Jurado et al., *Phys. Rev. Lett.* **93**, 072501 (2004).